6th European Conference on Computational Mechanics (ECCM 6)
7th European Conference on Computational Fluid Dynamics (ECFD 7)
11-15 June 2018, Glasgow, UK

# ON THE MULTIDIMENSIONAL ROE-LIKE LINEARIZATION FOR NON-EQUILIBRIUM MULTI-SPECIES GAS MIXTURES: APPLICATION TO RESIDUAL DISTRIBUTION SCHEMES

JESÚS GARICANO-MENA[1,*], PABLO SOLANO-LÓPEZ[1] AND GÉRARD DEGREZ[2]

[1] E.T.S. Ingeniería Aeronáutica y del Espacio, Universidad Politécnica de Madrid
Plaza del Cardenal Cisneros, 3, Madrid, 28040, España
[2] Service Aéro-Thermo-Mécanique, Université Libre de Bruxelles,
Avenue F. D. Roosevelt, 50, Bruxelles, 1050, Belgique
[*] Corresponding author: J. Garicano-Mena, jesus.garicano.mena@upm.es

**Key words:** residual distribution schemes, hypersonic flow, thermo-chemical non-equilibrium, conservative linearization, contour-integration based residual distribution schemes

**Abstract.** This contribution revolves around the procedure that Liu and Vinokur proposed to derive a Roe-like linearization for flows out of thermo-chemical equilibrium. More specifically, we consider the multidimensional generalization by Degrez and van der Weide and its application to residual distribution schemes. The multidimensional linearization is described in detail, and the conditions under which it is well defined are investigated. We show that the multidimensional generalization can be ill-defined under certain conditions; an alternative to handle shocked hypersonic flow fields in thermo-chemical non-equilibrium is proposed.

## 1 INTRODUCTION

Degrez and van der Weide introduced in 8 an strategy to generalize to the multidimensional case the Roe-like linearization procedure that Liu and Vinokur proposed in 22.
Liu and Vinokur's technique offered, in the context of approximated Riemann solvers, an effective method to derive a Roe-like *averaged* state $\vec{Z}_{avg}$ for which the so-called *property U* (see 27) was respected.
The significance of being able to compute an average state respecting property $U$ is precisely the guarantee that a linearized description of the Riemann problem will provide a solution consistent with that of the original non-linear problem, namely that the numerical algorithm will be able to -in the words of Roe- *"recognize a shock wave"* 27.
Liu and Vinokur's accomplishment was to offer Roe-like averaged states $\vec{Z}_{avg}$ under conditions for which the existence of such averages was not guaranteed to exist, namely for complex, highly non-linear thermodynamic models *e.g.* those used for two-phase or thermo-chemical non-equilibrium ($TCNEQ$) flows. References 32, 33 illustrate the usage of Liu and Vinokur's generalized Roe average for combustion applications.
Note that most of the of the applications employing the generalized Roe average apply it on a dimension-by-dimension basis. Seeking to take advantage of the multidimensional upwind residual distribution algorithms described in 34, Degrez and van der Weide devised an strategy to extend the linearization to the multidimensional case.

This contribution is structured as follows: the system of equations and the thermo-chemical model describing the flows of our interest are presented immediately after this introductory section. Section 3 offers then a brief introduction to Residual Distribution techniques, focusing specially in the computation and distribution of convective residuals. Next, the extension of the Roe-Liu-Vinokur linearization to the multidimensional case proposed by 8 is described in detail in section 4: special attention is paid to the conditions under which this extension is well-defined. In an attempt to unclutter as much as possible the exposition, appendix A contains additional details about handling source term residuals, and the solution procedure of the discrete nodal equations.

## 2 GOVERNING EQUATIONS

In this work we will consider inviscid *NEQ* flows including vibrational excitation and chemical reaction processes, which we will describe by means of a $n_S$ species (with $n_S \geq 2$), two temperatures model 24. These models assume that translational and rotational contributions to the internal energy are fully excited and in equilibrium at temperature $T$, while the vibrational and electronic modes are themselves in equilibrium at a temperature $T^v$ possibly different from $T$. In particular we will employ the equations presented in 14, particularized for the non-ionized case[1].

The set of equations describing the flow of an inviscid $n_S$ species, electrically neutral gas mixture, possibly reacting and/or under vibrational non-equilibrium conditions reads in compact vector form as:

$$\frac{\partial \vec{U}}{\partial t} + \nabla \cdot \bar{\bar{F}}^c = \vec{S}. \tag{1}$$

Here $\vec{U}$ stands for the vector of conserved variables and tensors $\bar{\bar{F}}^c$ collects the convective fluxes of the conserved quantities, while vector $\vec{S}$ contains the chemical and internal energy modes source terms. For a *TCNEQ* flow the vector of conserved variables is:

$$\vec{U} = [\rho_s, \quad \rho u_j, \quad \rho E, \quad \rho e^v]^t, \tag{2}$$

and therefore $n_{Eqs} = n_S + n_D + 2$. System of equations 1 expresses the conservation of mass (at the species level, and globally), momentum and energy (both total and vibrational) principles. In system above, $\rho_s$ stands for the density of the $s$-th species, while $\rho\vec{u}$, $\rho E$ and $\rho e^v$ are respectively the momentum, the total energy and the electronic-vibrational energy per unit volume. Additionally, $p$ is the pressure exerted by the mixture and $H$ is the specific total enthalpy.
The convective tensor is defined as (Einstein convention applies) $\bar{\bar{F}}^c = \vec{F}^c_j \cdot \vec{e}^t_j$ for $j \in \{x_1, \ldots, x_{n_D}\}$. Note that the vectors employed fulfill $\vec{U},\ \vec{F}^c_j,\ \vec{S} \in \mathbb{R}^{n_{Eqs}}$ and $\{\vec{e}_j\}$ is the canonical basis for $\mathbb{R}^{n_D}$. The mass production term for a given species $s$:

$$\frac{\dot{\omega}_s}{M_s} = \sum_{reactions} (\nu''_{s,r} - \nu'_{s,r}) \left\{ k_{r,f} \prod_{species} \left(\frac{\rho_k}{M_k}\right)^{\nu'_{k,r}} - k_{r,b} \prod_{species} \left(\frac{\rho_k}{M_k}\right)^{\nu''_{k,r}} \right\}. \tag{3}$$

Here $k_{r,f}$ and $k_{r,b}$ stand for the forward and backward reaction rates for the $r-th$ reaction; $\nu'_{k,r}$ and $\nu''_{k,r}$ are the stoichiometric coefficients and $M_k$ is the molar weight for the $k$-th species.

[1]Since a consistent treatment of charged species would require to couple the Maxwell equations to the model described here.

In this work, the $N$-$N_2$ gas mixture will be considered. Therefore, for a two-dimensional *TC-NEQ* (or *CNEQ*) flow computation, the number of conserved variables is 6 (or 5).
Finally, the term $\Omega^v$, in the case of gas mixtures involving only neutral species (i.e. in absence of ionization) accounts for the energy exchange (relaxation) between translational and vibrational modes and for the energy gained through dissociation or recombination processes:

$$\Omega^v = \sum_{s=1}^{n_S} \rho_s \frac{e^*_{v,s} - e_{v,s}}{\tau_s} + \sum_{s=1}^{n_S} \hat{D}_s \dot{\omega}_s. \tag{4}$$

The model is not closed until initial/boundary conditions, properties $k_{r,f}$, $k_{r,b}$, $\tau_s$ and an equation of state is provided. Due to space limitations we will cover here only parts of the thermodynamic model, and will encourage the reader to consults references 3, 16 for a detailed discussion on what are physically adequate initial/boundary conditions for the system of non-linear partial differential equations in Eqs. (1); and to 17, 14, 23 for an account on the calculation of all chemistry, thermodynamics and energy transfer properties.
At the equation of state level, the ideal gas law for a thermally perfect gas ($PG$) applies to each of the components of the gas mixture, which exert a *partial* pressure given by $p_s = {}^{R}/_{M_s}\rho_s T$. Here, $R$ is the universal gas constant $R = 8314.4^{J}/_{K\,kmol}$ and $M_s$ the $s$-th species molecular weight (in ${}^{kg}/_{kmol}$). The total pressure of the mixture is:

$$p = \sum_{s=1}^{n_S} p_s. \tag{5}$$

Specific enthalpy $H$ relates to pressure as $H = E + {}^{p}/_{\rho}$. Total energy $\rho E$ and pressure $p$ of the mixture can be further related if one realizes that $\rho E$ includes contributions from the translational-rotational modes, from the vibrational-electronic modes and from the kinetic energy, as in $\rho E = \rho e^{tr} + \rho e^{v} + \frac{1}{2}\,\rho \vec{u}^t \cdot \vec{u}$. Each of these gathers in turn contributions from the different species in the mixture:

$$\rho e^{tr} = \sum_{s=1}^{n_S} \rho_s e^{tr}_s,\ \rho e^{v} = \sum_{s=1}^{n_S} \rho_s e^{v}_s,\ \frac{1}{2}\,\rho \vec{u}^t \cdot \vec{u} = \sum_{s=1}^{n_S} \rho_s \frac{\|\vec{u}\|^2}{2}.$$

The $s$-th species translational-rotational energy is $e^{tr}_s = \int_{T^0}^{T} C^{tr}_{v,s}\, d\tau + h^0_s$; $h^0_s$ is the formation enthalpy of the species at the reference temperature $T^0$ and $C^{tr}_{v,s}$ is the translational-rotational specific heat at constant volume. Since the components of the mixture behave as calorically perfect gases, $C^{tr}_{v,s} = \frac{3}{2}\,R_s$ for monoatomic species and $\frac{5}{2}\,R_s$ for diatomic molecules.
The expression for the $s$-th species vibrational energy $e^v_s$ is derived under the assumption that the internal quantum states are populated according to a Boltzmann distribution, so molecular species behave as harmonic oscillators. Therefore $e^v_s = 0$ for atomic species and $e^v_s = \frac{R}{M_s}\frac{\theta^v_s}{e^{\theta^v_s/T^v}-1}$ for diatomic molecules; $\theta^v_s$ is a characteristic vibrational temperature for the $s$-th species.
Differentiating Eq. (5) and algebraic manipulation, see Ref. 22, leads to:

$$d\,p = \sum_{s=1}^{n_S} \gamma_s\, d\rho_s + \beta\, d\rho e^{tr}. \tag{6}$$

Terms $\gamma_s$ and $\beta$ in Eq. (6) stand respectively for the partial derivatives of pressure with respect to the translational-rotational energy and the species densities ; they are given by:

$$\beta = \frac{\partial p}{\partial \rho e^{tr}} = \frac{\sum_{s=1}^{n_S} y_s {}^{R}/_{M_s}}{\sum_{s=1}^{n_S} y_s C^{tr}_{v,s}},\ \text{ and }\ \gamma_s = \frac{\partial p}{\partial \rho_s} = {}^{R}/_{M_s} T - \beta e^{tr}_s, \tag{7}$$

where term $y_s \equiv \rho_s/\rho$ is the mass fraction of $s$-th species. Pressure derivatives $\gamma_s$ and $\beta$ intervene as well in the expression for the frozen speed of sound:

$$a^2 = \sum_{s=1}^{n_S} y_s \gamma_s + \left( h - e^v - \frac{\|\vec{u}\|^2}{2} \right) \beta = (1+\beta)\,\frac{p}{\rho}. \tag{8}$$

## 3 RESIDUAL DISTRIBUTION TECHNIQUES

In this section, we briefly introduce the *RD* discretization for the system of equations (1) by reviewing the main concepts from references 34, 25, 29. Assume we intend to solve Equation (1) on a simplicial tessellation $\Omega^h$ of the spatial domain $\Omega$. Let us denote by $n_{Elem}$ and $n_{DoF}$ the number of *simplices* (triangles in `2D`, tetrahedra in `3D`) and vertices in $\Omega^h$. The numerical solution to Eq. (1), $\vec{U}^h$ [2] can be immediately expanded in terms of the associated nodal basis functions $N_l \in P^1\left(\Omega^h\right)$, see Fig. 1:

$$\vec{U}^h(\vec{x},t) = \sum_{j=1}^{N_{DOF}} \vec{U}_j(t)\, N_j(\vec{x}) \tag{9}$$

where the nodal basis functions $N_j$ fulfill $N_j(\vec{x}_k) = \delta_{jk}$.

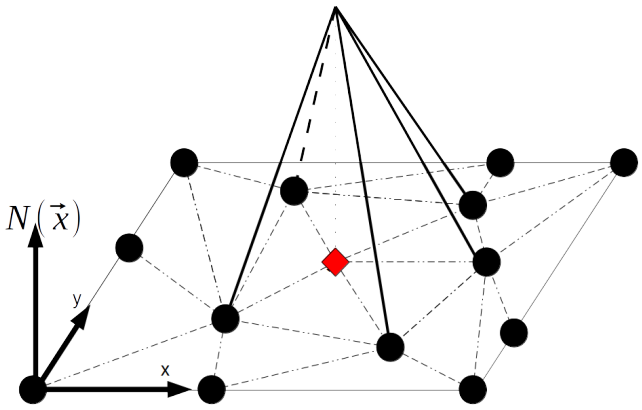


Figure 1: $P1$ nodal base function for $l$-th node.

The steady state residual for element $\Omega$ is defined as:

$$\vec{\Phi}^{\Omega} = \int_{\Omega} \left( \frac{\partial \vec{F}_j^c}{\partial x_j} - \vec{S} \right) dv = \vec{\Phi}^{c,\Omega} - \vec{\Phi}^{S,\Omega}, \tag{10}$$

and gathers contributions from the convective and source terms.
An equation for each of the nodal *DoF*'s is obtained by distributing fractions of the cell residuals $\vec{\Phi}^{\Omega}$ to the nodes forming part of the cell:

$$\vec{\Phi}_l = \sum_{\Omega_i \in \Xi_l} \vec{\Phi}_l^{\Omega_i} = \sum_{\Omega_i \in \Xi_l} \left( \mathfrak{f}^c\left(\vec{\Phi}^{c,\Omega_i}\right) + \mathfrak{f}^S\left(\vec{\Phi}^{S,\Omega_i}\right) \right). \tag{11}$$

[2] Superscript $h$ marks here the solution obtained as a numerical approximation. Unless we want to insist on this fact, we will often drop the superscript.

Different choices for the functionals $\mathfrak{f}^c$ and $\mathfrak{f}^S$ above define the different schemes employed. In this section we deal with the computation and distribution of the convective residuals, deferring the treatment of the source term contributions, together with the solution strategy to Appendix A.

### 3.1 Convective residual

The convective contribution to the nodal equation of the cell residual is expressed generically as:

$$\vec{\Phi}_l^c = \sum_{\Omega_i \in \Xi_l} B_l^{\Omega_i} \left( K_j^+, K_j^- \right) \cdot \vec{\Phi}^{c,\Omega_i}, \tag{12}$$

in terms of the so called distribution matrices $B_l^{\Omega_i}$; these matrices depend in turn on the nodal upwind parameters $K_j$, described in section 3.1.1.
*RD* schemes can be classified according to how the convective residual is computed: we distinguish among linearization-based (*LRD*) and contour-integration-based (*CRD*) schemes. In this contribution we focus mainly on *LRD* schemes; references 4, 20 provide extensive details on *CRD* techniques.

#### 3.1.1 Computing the advective residual: *LRD vs CRD*

Assume that one can find a variable set $\vec{Z}$ such that both the unknown $\vec{U}$ and the flux vector $\vec{F}_j^c$ can be expressed as a polynomial on the components of $\vec{Z}$ of $2^{nd}$ degree at most. In that case, by linearizing $\vec{F}_j^c$ we obtain:

$$\vec{\Phi}^{c,\Omega_i} = \int_{\Omega_i} \frac{\partial \vec{F}_j^c}{\partial x_j} dv = \int_{\Omega_i} \frac{\partial \vec{F}_j^c}{\partial \vec{Z}} \frac{\partial \vec{Z}}{\partial x_j} dv.$$

Since the solution is expressed in $P1$ (*linear*) elements, we have:

$$\left. \frac{\partial \vec{Z}}{\partial x_j}^h \right|_{\Omega_i} = const \text{ and } \vec{\Phi}^{c,\Omega_i} = \left( \int_{\Omega_i} \frac{\partial \vec{F}_j^c}{\partial \vec{Z}} dv \right) \left. \frac{\partial \vec{Z}}{\partial x_j}^h \right|_{\Omega_i}.$$

At the same time, the Jacobian $\frac{\partial \vec{F}_j^c}{\partial \vec{Z}}$ is a linear function and henceforth the following:

$$\int_{\Omega_i} \frac{\partial \vec{F}_j^c}{\partial \vec{Z}} dv = \Omega_i \frac{\partial \vec{F}_j^c}{\partial \vec{Z}} \left( \vec{U} \left( \vec{Z}_{avg} \right) \right),$$

holds *exactly*. The exact value of $\vec{\Phi}^{c,\Omega_i}$ is therefore given by the simple relation:

$$\vec{\Phi}^{c,\Omega_i} = \Omega_i \frac{\partial \vec{F}_j^c}{\partial \vec{Z}} \left( \vec{U} \left( \vec{Z}_{avg} \right) \right) \left. \frac{\partial \vec{Z}}{\partial x_j}^h \right|_{\Omega_i}. \tag{13}$$

Eq. (13) can be rewritten more conveniently taking an intermediate step:

$$\vec{\Phi}^{c,\Omega_i} = \underbrace{\frac{\partial \vec{F}_j^c}{\partial \vec{U}} \left( \vec{U}_{avg} \right)}_{A_j^{c,U}} \frac{\partial \vec{U}}{\partial \vec{Z}} \left( \vec{U}_{avg} \right) \sum_{k \in \Omega_i} \frac{1}{2\Omega} \vec{Z}_k n_{j,k},$$

where we have introduced $A_j^{c,U}$, the Jacobian of the advective flux function $\vec{F}_j^c$ with respect to the conserved variables $\vec{U}$. The consistent conservative states are defined as:

$$\vec{U}_k^{Consistent} \equiv \frac{\partial \vec{U}}{\partial \vec{Z}}\left(\vec{U}_{avg}\right)\vec{Z}_k, \text{ with } k \in \{1,\ldots,n_D+1\},$$

and the final expression for $\vec{\Phi}^{c,\Omega_i}$ is:

$$\vec{\Phi}^{c,\Omega_i} = \sum_{k\in\Omega_i} \underbrace{\frac{1}{n_D} A_j^{c,U} n_{j,k}}_{K_k} \vec{U}_k^{Consistent}. \tag{14}$$

This reformulation brings forward the so-called nodal upwind parameters $K_k$:

$$K_k = \frac{1}{n_D} A_{x_d}^{c,U}\, n_{x_d,k}, \text{ and } k \in \{1,\ldots,n_D+1\}, \tag{15}$$

where $A_{x_d}^{c,U}$ is the Jacobian of the advective flux along direction $x_d$, $n_{j,x_d}$ are the components of the vectors normal to the element faces and $n_D$ is the dimensionality of the problem. Most *RD* schemes are formulated in terms of theses $K_k$, *cf.* section 3.1.2.

A linearization procedure as described above is possible if $\frac{\partial F_j^c}{\partial \vec{Z}}$ and $\frac{\partial \vec{U}}{\partial \vec{Z}}$ are linear functions of $\vec{Z}$, and this depends ultimately on the equation of state of the thermodynamic model employed. For the perfect gas model, such a linearization is available: the Roe linearization introduced in 27, developed originally for dimensionally splitted *FV* methods. Later on, Deconinck *et al.* extended the linearization procedure to the multi-dimensional *RD* framework, 5.

Unfortunately, for the *NEQ* models considered in this work, a $\vec{Z}$ variable is not readily available. However, Degrez and van der Weide, building upon Liu and Vinokur's ideas 22, proposed a linearization procedure circumventing this limitation in 8. We describe their linearization strategy in section 4 in detail, and provide evidence that it breaks down under certain circumstances.

There is yet another alternative approach whenever a $\vec{Z}$ variable cannot be defined: the element residual evaluation $\vec{\Phi}^{c,\Omega_i}$ and its distribution can be done independently (see 4, 30) as long as $\vec{\Phi}^{c,\Omega_i}$ respects second equality in flux conservation and the distribution coefficients employed respect the consistency condition:

$$\sum_{l\in\Omega_i} B_l^{\Omega_i} = \bar{\bar{I}}_{nEqs}, \tag{16}$$

where no matter which inconsistent average state $\vec{U}_{avg,*}$ can be employed to define the distribution matrices $B_l^{\Omega_i}$. Residual Distribution reformulations exploiting this approach are termed *Contour-Integration* (*CRD*, 4, 25) or *Flux Quadrature* (*FQ-RD*, 29) schemes.

As for the actual evaluation of the element residual, it is enough that integral:

$$\vec{\Phi}^{c,\Omega_i} = \int_{\Omega_i} \nabla\cdot\vec{F}_j^c dv = \oint_{\delta\Omega_i} \vec{F}_j^c \vec{1}_j^{ext} ds,$$

is evaluated with an error lower than the distribution error. In this work we follow the approach in 4 and evaluate the contour integral by numerical (Gauss) integration:

$$\vec{\Phi}^{c,\Omega_i} = \oint_{\delta\Omega_i} \vec{F}_j^c \vec{1}_j^{ext} ds = \sum_{f=1}^{n_D+1} \int_{S_f} \vec{F}_j^c \vec{1}_j^{ext} ds = \sum_{f=1}^{n_D+1} \sum_{q\in QP} \omega_q \left(\vec{F}_j^c \vec{1}_j^{ext}\right)_q l_q, \tag{17}$$

where the sum indexed by $q$ extends over the quadrature points on each of the element faces (edges in `2D`).

### 3.1.2 Distributing the advective residual: matrix *RD* schemes

The convective contribution to the nodal equation of the cell residual (namely, the distributive functional $\mathfrak{f}^c$) in Eq. (11) is expressed generically as :

$$\vec{\Phi}_l^c = \sum_{\Omega_i \in \Xi_l} B_l^{\Omega_i} \left(K^{\pm}\right) \cdot \vec{\Phi}^{c,\Omega_i}, \tag{18}$$

in terms of the so called distribution matrices $B_l^{\Omega_i}$, which depend in turn on the upwind parameters introduced in Eq. (15). Notice that these can be factorized as (see appendix A):

$$K_k = \frac{1}{n_D} A_j^{c,U} \, n_{j,k} = \frac{1}{n_D} R_k^U \cdot \Lambda_k \cdot L_k^U. \tag{19}$$

where $\Lambda_k$ is the diagonal matrix containing the eigenvalues of the projected advective Jacobian, and $R_k/L_k$ are matrices whose columns/rows are the right/left eigenvectors of $K_k$. Splitting the positive and negative parts of $\Lambda_l$ as $\Lambda_l^+/\Lambda_l^-$, we finally obtain:

$$K_l^{\pm} = \frac{1}{n_D} R_l^U \cdot \Lambda_l^{\pm} \cdot L_l^U. \tag{20}$$

Matrix $|K_l|$ is simply obtained as $|K_l| \equiv K_l^+ - K_l^- = \frac{1}{n_D} R_l^U \cdot \left(\Lambda_l^+ - \Lambda_l^-\right) \cdot L_l^U$.
We present now several *RD* schemes and discuss their properties.

#### Low diffusion A scheme

Introduced in 31, the distribution matrix for system of equations 34 is:

$$B_l^{\Omega_i, LDA} = (K_l)^+ \cdot \left( \sum_j (K_j)^+ \right)^{-1}. \tag{21}$$

This scheme is linear, preserves linear solutions and is multidimensional upwind. It is probably the most used *RD* scheme for the simulation of smooth flow fields.

#### Narrow scheme

The scalar $N$ was devised by Roe in 26, and reformulated as a matrix *RD* scheme in 34. The $N$ scheme contribution to the nodal residual is given by:

$$\vec{\Phi}_l^{c,\Omega_i,N} = K_l^+ \cdot \left(\vec{U}_l - \vec{U}_{inlet}^{\Omega_i}\right). \tag{22}$$

where the *inlet* state $\vec{U}_{inlet}^{\Omega_i}$ reads:

$$\vec{U}_{inlet}^{\Omega_i} = \left( \sum_{j \in \Omega_i} K_j^- \right)^{-1} \cdot \sum_{j \in \Omega_i} K_j^- \cdot \vec{U}_j. \tag{23}$$

The $N$ scheme is linear, multi-dimensional upwind and *positive*; hence it is only $1^{st}$ order accurate. Notice how a distribution matrix cannot be obtained explicitly for the system $N$ scheme. There is an important relationship between the $N$ and the $LDA$ schemes, namely that $N$ scheme is precisely the $LDA$ scheme supplemented by an additional dissipative term $\vec{\delta}_l^{Diss,N}$ of crosswind nature 4, 25:

$$\vec{\Phi}_l^{c,\Omega_i,N} = \vec{\Phi}_l^{c,\Omega_i,LDA} + \vec{\delta}_l^{Diss,N}. \tag{24}$$

Concerning the $CRD$ variant, the $Nc$ scheme is given by:

$$\vec{\Phi}_l^{c,\Omega_i,Nc} = \vec{\Phi}_{l,*}^{c,\Omega_i,N} - B_l^{\Omega_i,LDA}\delta\vec{\Phi}^c, \tag{25}$$

where $\vec{\Phi}_{l,*}^{c,\Omega_i,N}$ is the result of the inconsistent evaluation of Eq. (22) and $\delta\vec{\Phi}^c$ is the difference between the residual computed with Eq. (14) (also an inconsistent quantity) and the residual given by Eq. (17):

$$\delta\vec{\Phi}^c = \vec{\Phi}_{\Omega,*}^c\Big|_{Inconsistent} - \vec{\Phi}_{\Omega}^c\Big|_{Gauss} = \sum_{j\in\Omega_i} K_j\vec{U}_j - \vec{\Phi}_{\Omega}^c\Big|_{Gauss}. \tag{26}$$

Relation (24) holds for the $Nc$-$LDAc$ pair as well. There is, nevertheless, an important difference between the original $N$ scheme and its $CRD$ variant: the $Nc$ scheme is non-positive, meaning that the capture of certain shock waves may present oscillations. This is not a concern for $PG$ simulations, as long as one uses the Roe-Struijs-Deconinck linearization variable $\vec{Z}$, (in that case $Nc$ and $N$ schemes coincide). The lack of monotonicity is, however, specially problematic for $NEQ$ flows whenever strong, bow shock waves are present in the domain; this is precisely the case when the $\vec{Z}$ variable is less likely to be well-defined, see section 4). The underlying reason is the mass production terms -Eq. (3)- highly non-linear dependence on temperature: the extreme variations in temperature across the numerically captured shock wave result in unphysical production/destruction of species, and this leads eventually to simulation blow up 12, 13, 10.

**Blended schemes**

A family of non-linear schemes can be obtained from a weighted averaging of $N$ and $LDA$ schemes (or its $CRD$ counterparts):

$$\vec{\Phi}_l^{c,\Omega_i,B} = \Theta^{\Omega_i}\vec{\Phi}_l^{c,\Omega_i,N} + \left(\bar{\bar{I}}_{nEqs} - \Theta^{\Omega_i}\right)\vec{\Phi}_l^{c,\Omega_i,LDA}, \tag{27}$$

The resulting scheme is therefore multi-dimensional upwind, positive and linearity preserving. Many variants can be constructed 6, 9, 29, 13 depending on the choice of $\Theta^{\Omega_i}$. We will use the shock detector function in Garicano-Mena et al. 13
Relation (24), when substituted into equation (27) leads to:

$$\vec{\Phi}_l^{c,\Omega_i,B} = \vec{\Phi}_l^{c,\Omega_i,LDA} + \theta\vec{\delta}_l^{Diss,N}. \tag{28}$$

Recall term $\vec{\delta}_l^{Diss,Nc}$ is non-positive, and hence oscillations across the shock wave may appear for $NEQ$ flows. A straightforward strategy to attenuate these oscillations is simply to supplement the cross-wind term $\vec{\delta}_l^{Diss,Nc}$ with additional dissipation, as in:

$$\vec{\Phi}_l^{c,\Omega_i,B} = \vec{\Phi}_l^{c,\Omega_i,LDA} + \theta\left(\vec{\delta}_l^{Diss,N} + \vec{\delta}_l^{Diss,D}\right). \tag{29}$$

In this work we employ as additional dissipation term that of the simple Lax-Friedrichs scheme 21,which can be recast in $RD$ form as (see 1):

$$\vec{\delta}_l^{Diss,LxF} = \max_{k\in\Omega_i} |\lambda_k| \sum_{m\in\Omega_i} \left(\vec{U}_l - \vec{U}_m\right). \tag{30}$$

where $\lambda_k$ are the eigenvalues of $K_l$. Alternatives to design physically based shock-capturing terms $\vec{\delta}_l^{Diss,D}$ are provided in 11.

## 4 THE MULTIDIMENSIONAL ROE-LIU-VINOKUR LINEARIZATION IN 8

Degrez and van der Weide presented in 8 a strategy to derive a multidimensional linearization variable $\vec{Z}$ guaranteeing conservation at the discrete level when simulating $CNEQ$ flows. Here we extend the technique for the $TCNEQ$ case, and analyze the implications of its application.

### 4.1 Description of the linearization procedure

Following the path traced by Degrez, we define the variable $\vec{Z} \equiv \left[\sqrt{\rho}\vec{Y}^t_{n_S\times 1}, \quad \sqrt{\rho}\vec{u}^t, \quad \sqrt{\rho}H, \quad \sqrt{\rho}e^v\right]^t$. The convective flux vector for the $TCNEQ$ case can be splitted as:

$$\vec{F}_j^c = \underbrace{\left(\vec{F}_j^c - [\vec{0}_{n_S x1}, p\vec{1}_j, 0, 0]^t\right)}_{\vec{Q}} + \underbrace{[\vec{0}_{n_S x1}, p\vec{1}_j, 0, 0]^t}_{\vec{\Pi}}. \tag{31}$$

Observe how all terms in $\vec{Q}$ can be expressed as quadratic functions of the components of $\vec{Z}$, and thus entries in $\frac{\partial \vec{F}_j^c}{\partial \vec{Z}}$ are just linear functions. On the other hand $\vec{\Pi}$ just contains the pressure. But more than in pressure itself, we are interested in its differential; Eq. (6) provides:

$$dp = \sum_{s=1}^{n_S} \gamma_s \, d\rho_s + \beta \, d\rho e^{tr}. \tag{32}$$

In order to employ this principle in a multidimensional upwind framework, we rather consider relation Eq. (32) at the gradient level:

$$\nabla p = \sum_{s=1}^{n_S} \gamma_s \, \nabla\rho_s + \beta \, \nabla\rho e^{tr}, \tag{33}$$

which can be immediately recast in terms of the components of parameter vector $\vec{Z}$ by using the relation:

$$\rho e^{tr} = \rho H - \frac{\rho\vec{u}^t \cdot \vec{u}}{2} - \rho e^v - p, \tag{34}$$

and considering $\rho_s = \left(\sum_{r=1}^{n_S} \sqrt{\rho}y_r\right)\sqrt{\rho}y_s$, $\rho\vec{u}^t \cdot \vec{u} = \sqrt{\rho}\vec{u}^t \cdot \sqrt{\rho}\vec{u}$, $\rho H = \left(\sum_{r=1}^{n_S} \sqrt{\rho}y_r\right)\sqrt{\rho}H$, and $\rho e^v = \left(\sum_{r=1}^{n_S} \sqrt{\rho}y_r\right)\sqrt{\rho}e^v$.

At this point, if one manages to find values for $\gamma_s$ and $\beta$ for which Eq. (33) holds, then the gradient of pressure will be defined in terms of $\vec{Z}$, making in turn $\frac{\partial\vec{\Pi}}{\partial\vec{Z}}$ a linear function of the

parameter vector as well: therefore evaluating $A_j^{c,U}$ at an averaged state $\vec{Z}_{avg}$, would provide a conservative convective residual.
The problem is, however, that Eq. (33) provides only as many equations as the dimensionality $n_D$ of the problem (namely 1, 2 or 3) while $n_S + 1$ parameters have to be defined for the case of a non-ionized $n_S$ species gas mixture.
In order to determine these $n_S + 1$ parameters, we can interprete Eq. (33) as $n_D$ restrictions[3]:

$$r_j \equiv \frac{\partial p}{\partial x_j}\,\beta - \sum_{s=1}^{n_S} \frac{\partial \rho_s}{\partial x_j}\,\gamma_s - \frac{\partial \rho e^{tr}}{\partial x_j},\;\; j = 1 \dots n_D, \tag{35}$$

that the solution we seek for should respect in order to guarantee conservation. In that case, it would be sensible to look for a solution which, while fulfilling the aforementioned restrictions (guaranteeing thus conservation), is the closest one to a given a priori approximation, like for example the nodal averages:

$$\hat{\gamma}_s = \sum_{i=1}^{n_D+1} \frac{\gamma_s|_i}{n_D+1} \quad \hat{\beta} = \sum_{i=1}^{n_D+1} \frac{\beta|_i}{n_D+1}. \tag{36}$$

Under these hypotheses, we are faced with a constrained minimization problem. According to 22, in order not to obtain a solution dependent on the arbitrary reference enthalpy entering in the definition of the parameters $\gamma_s$, it is better to work on the space $\{\xi_1, \dots, \xi_N; \omega\}$, where $\xi_s = \gamma_s/\beta$, $s = 1, \dots, n_S$ and $\omega = 1/\beta$.
We can define then the Lagrangian for the restricted minimum distance problem:

$$\mathcal{L} \equiv (\omega - \hat{\omega})^2 + \frac{1}{\hat{\sigma}^2} \sum_{s=1}^{n_S} \left(\xi_s - \hat{\xi}_s\right)^2 - \vec{\lambda}^t \cdot \left(\nabla p\,\omega - \sum_{s=1}^{n_S} \nabla \rho_s\,\xi_s - \nabla \rho e^{tr}\right). \tag{37}$$

Factor $\hat{\sigma}^{-2}$ is included for dimensional consistency, and $\hat{\sigma}$ taken as the local speed of sound. The corresponding stationarity conditions are:

$$\begin{aligned}
\frac{\partial \mathcal{L}}{\partial \xi_r} &= \frac{2}{\hat{\sigma}^2}\left(\xi_r - \hat{\xi}_r\right) + \vec{\lambda}^t \cdot \nabla \rho_r = 0,\;\; r = 1 \dots n_S, \\
\frac{\partial \mathcal{L}}{\partial \omega} &= 2\,(\omega - \hat{\omega}) - \vec{\lambda}^t \cdot \nabla p = 0, \\
\frac{\partial \mathcal{L}}{\partial \lambda_j} &= \frac{\partial p}{\partial x_j}\,\beta - \sum_{s=1}^{n_S} \frac{\partial \rho_s}{\partial x_j}\,\gamma_s - \frac{\partial \rho e^{tr}}{\partial x_j},\;\; j = 1 \dots n_D.
\end{aligned} \tag{38}$$

Fig. 2 shows the graphical interpretation of the minimization problem defined by the Lagrangian in Eq. (37) for a $2D$ computation and a 2 species mixture: starting from an approximation $\hat{P}$ in the space $\{\xi_r; \omega\}$, we look for the closest point $\tilde{P}$ which fulfills at the same time the $n_D = 2$ restrictions, that is, lies on the line where the blue and the green planes intersect.

[3]Here, the $\frac{\partial}{\partial x_j}$ operator applied to pressure is the discrete *FE* one $\left.\frac{\partial p}{\partial x_j}\right|^h = \frac{1}{2}\sum_{k=1}^{n_D+1} p_k n_{j,k}$. The same operator applied to other magnitude $m$ should be understood as a *consistent* gradient $\left.\frac{\partial m}{\partial x_j}\right|^c = \left.\frac{\partial m}{\partial \vec{Z}}\right|_{\vec{Z}_{avg}} \cdot \left.\frac{\partial \vec{Z}}{\partial x_j}\right|^h$. When the context is clear, superscripts $h$ and $c$ will be omitted.

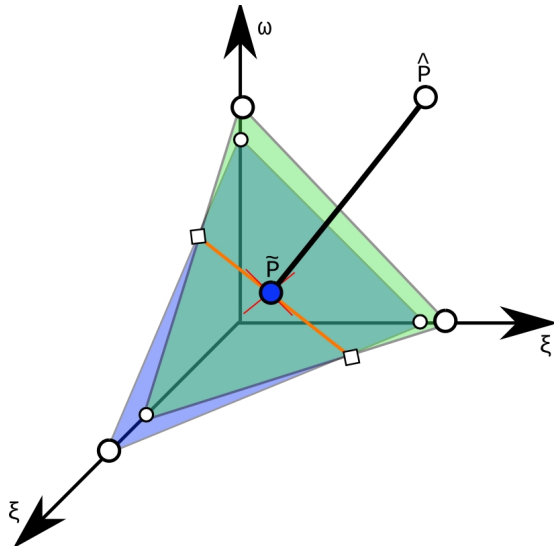


Figure 2: Constrained minimization problem: graphical interpretation.

The stationarity conditions Eq. (38) translate into a linear system of equations:

$$\mathcal{A} \cdot \vec{x} = \vec{b}, \tag{39}$$

which consists, after application of elemental operations, of the coefficient matrix $\mathcal{A}$:

$$\mathcal{A} = \left[\begin{array}{c|c|ccc} \bar{\bar{I}}_{n_S} & 0 & \frac{\hat{\sigma}^2}{2}\frac{\partial \rho \vec{Y}_{n_S\times 1}}{\partial x} & \frac{\hat{\sigma}^2}{2}\frac{\partial \rho \vec{Y}_{n_S\times 1}}{\partial y} & \frac{\hat{\sigma}^2}{2}\frac{\partial \rho \vec{Y}_{n_S\times 1}}{\partial z} \\ \hline \vec{0}_{1\times n_S} & 1 & -\frac{1}{2}\frac{\partial p}{\partial x} & -\frac{1}{2}\frac{\partial p}{\partial y} & -\frac{1}{2}\frac{\partial p}{\partial z} \\ \hline \vec{0}_{1\times n_S} & 0 & C_{xx} & C_{xy} & C_{xz} \\ \vec{0}_{1\times n_S} & 0 & C_{xy} & C_{yy} & C_{yz} \\ \vec{0}_{1\times n_S} & 0 & C_{xz} & C_{yz} & C_{zz} \end{array}\right], \tag{40}$$

of the vector of unknowns $\vec{x} = \vec{x} = \left[\xi_1, \ldots, \xi_N; \omega; \lambda_{x_j}\right]^t$ and of the forcing vector $\vec{b} = \left[\hat{\xi}_1, \ldots, \hat{\xi}_N; \hat{\omega}; -\hat{\omega}\,\delta p_{x_j}\right]^t$.

In Eq. (40), $C_{x_i\,x_j}$ stands for:

$$C_{x_i\,x_j} = \frac{1}{2}\left(\frac{\partial p}{\partial x_i}\frac{\partial p}{\partial x_j}\right) + \hat{\sigma}^2 \sum_{s=1}^{n_S}\left(\frac{\partial \rho_s}{\partial x_i}\frac{\partial \rho_s}{\partial x_j}\right), \tag{41}$$

while $-\hat{\omega}\delta p_{x_j}$ is:

$$\delta p_{x_j} = (1+\hat{\omega})\frac{\partial p}{\partial x_j} - \sum_{s=1}^{n_S}\frac{\partial \rho_s}{\partial x_j}\hat{\xi}_s - \frac{\partial \rho e^{tr}}{\partial x_j}. \tag{42}$$

The structure of the linear system in Eq. (39) is such that a $n_D \times n_D$ subsystem:

$$\mathcal{B}\vec{\lambda} = -\omega\vec{\delta p}, \tag{43}$$

can be decoupled. Provided one can invert $\mathcal{B}$, $\xi_s$ and $\omega$ are immediately obtained by back substitution:

$$\tilde{\omega} = \hat{\omega} + \frac{1}{2}\left(\lambda_x \frac{\partial p}{\partial x} + \lambda_y \frac{\partial p}{\partial y} + \lambda_z \frac{\partial p}{\partial z}\right), \text{ and } \tilde{\xi}_s = \hat{\xi}_s - \frac{\hat{\sigma}^2}{2}\left(\lambda_x \frac{\partial \rho_s}{\partial x} + \lambda_y \frac{\partial \rho_s}{\partial y} + \lambda_z \frac{\partial \rho_s}{\partial z}\right). \quad (44)$$

The values that are actually employed in the computation are obtained in a straightforward manner from $\tilde{\beta} = \frac{1}{\tilde{\omega}}$ and $\tilde{\gamma}_s = \tilde{\beta}\,\tilde{\xi}_s$.

It is evident that the success of the whole process revolves around the invertibility of $\mathcal{B}$. A priori one would expect this task to be relatively straightforward, $\mathcal{B}$ being a real symmetric matrix. However, when using the linearization procedure, we found more often than not values for $\tilde{\beta}$ and $\tilde{\gamma}_s$ that respect conservation at the discrete level (that is, with the restrictions $r_j$ equal to machine zero) but which correspond to unphysical situations ( *i.e.* $\tilde{\beta} < 0$ ).
Since the we have certain freedom to determine the pressure derivatives, the negative $\tilde{\beta}$ problem can be dealt with by setting $\tilde{\beta} = \hat{\beta}$ and determining the set of $\tilde{\gamma}_s$ by the same minimization procedure described above. In this manner, we have been able to solve a *NEQ* two jets problem. The problem consists in two uniform, supersonic $N$-$N_2$ streams discharging into a square domain. The conditions of each of the jets are given in Table 1.

Table 1: Testcase definition: *NEQ* two jets.

| | $Ma_\infty$ | $p_\infty\,(kPa)$ | $T_\infty = T_\infty^v\,(K)$ | $\rho_\infty\,(kg/m^3)$ | $y_{N,\infty}$ | $y_{N_2,\infty}$ |
|---|---|---|---|---|---|---|
| $y < 0.5$ | 2.4 | 10.3 | 1750 | 0.019824 | 0 | 1 |
| $y > 0.5$ | 4.7 | 5 | 3500 | 0.004809 | $6 \times 10^{-4}$ | 0.9994 |

We have computed this testcase both with the *LRD N* scheme and with the *CRD Nc* scheme. Fig. 3b shows the pressure field for the *LRD* solution. In Figure 5 we compare profiles of $p$, $T$ and $T_v$, $\rho$, $Ma$ and mass fractions along a constant $X$ section : both *LRD* and *CRD* solutions are nearly indistinguishable. The main difference lies however in the effort needed to obtain each of them when starting from an uniform flow field: on the one hand, the *CRD* solution needed to be initialized with an explicit pseudo-time stepping procedure; non-monotonicity of the *CRD* scheme resulted in temperature undershoots that were addressed by clipping temperature to $T_{min} = 200\,K$. Once the shock was in place, the *CRD* solution could be restarted in implicit mode, but maintaining the clipping active almost until convergence was achieved. On the other hand, the *LRD* solution converged easily to steady state, starting from the uniform flow field with the implicit strategy; $T$-clipping was never needed.
Unfortunately, when addressing more involved testcases, *i.e.* an inviscid *NEQ* ramp flow, the *LRD N* scheme does not converge, and sometimes even blows up. In the next section we investigate and propose an explanation for this behavior.

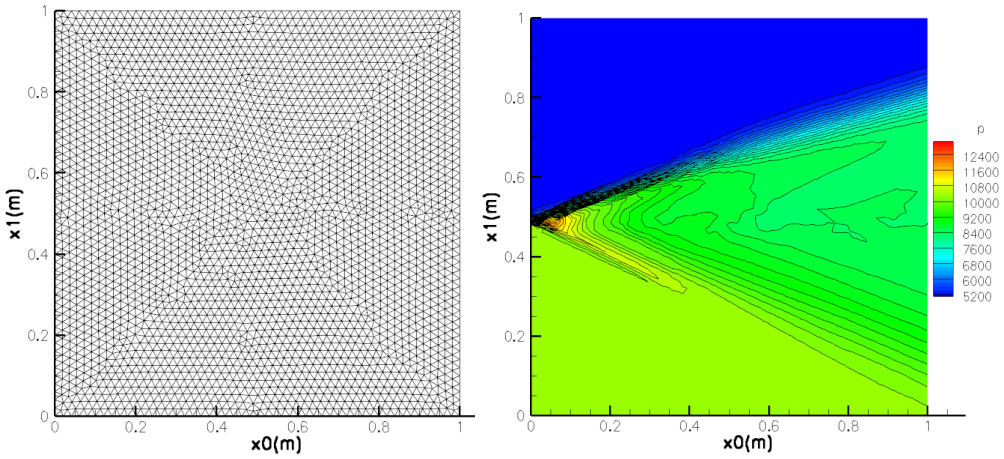


(a) Unstructured grid. (b) Pressure ($Pa$).

Figure 3: Two jets *NEQ* problem.

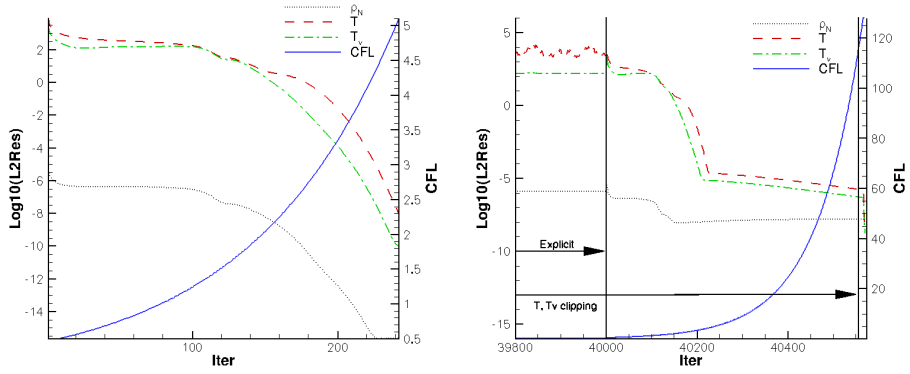


(a) *LRD* simulation. (b) *CRD* simulation.

Figure 4: Two jets *NEQ* problem: convergence histories.

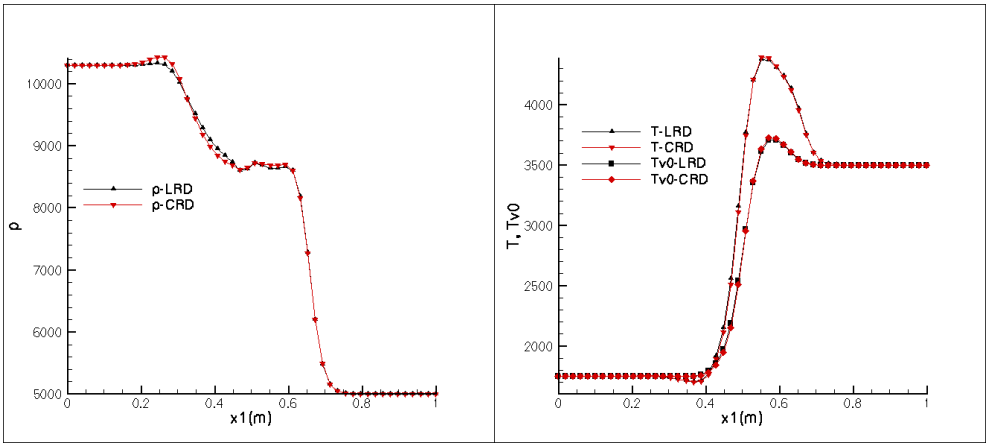


(a) Pressure ($Pa$). (b) $T$ and $Tv$ ($K$).

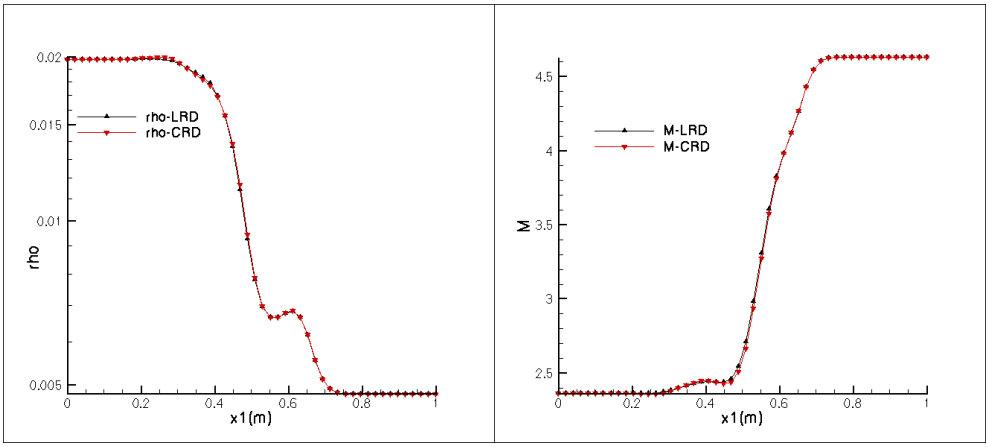


(c) Density ($kg/m^3$). (d) Mach number.

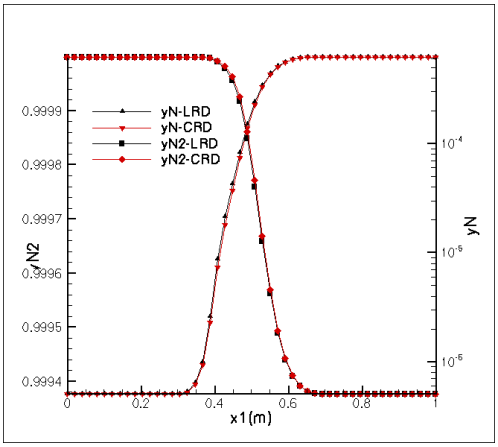


(e) Mass fractions.

Figure 5: Two jets $NEQ$ problem: section $x = 0.5\,m$.

### 4.2 Well-posedness of the *TCNEQ* Roe-like linearization

In previous section we pointed out that the success of the linearization procedure hinges on the invertibility of sub-matrix $\mathcal{B}$ in Eq. (43), which is symmetric and with real entries. Such matrices are possibly the most favourable case one could expect for ... assuming that the determinant of the matrix is not zero, of course!
In order to ease the analysis of the invertibility of $\mathcal{B}$ we introduce the vector:

$$\vec{w} = \left[ \frac{\hat{\sigma}}{\sqrt{2}} \rho \vec{Y}_{n_S \times 1} \frac{1}{\sqrt{2}} p \right], \tag{45}$$

and the following matrix:

$$\nabla \vec{w} = \left[ \begin{array}{c} \frac{\partial}{\partial x} \\ \frac{\partial}{\partial y} \\ \frac{\partial}{\partial z} \end{array} \right] \cdot \left[ \frac{\hat{\sigma}}{\sqrt{2}} \rho \vec{Y}_{n_S \times 1} \frac{1}{\sqrt{2}} p \right] \equiv M \in \mathcal{M}_{n_D \times N} \text{ with } N = n_S + 1. \tag{46}$$

The whole minimization problem in Eq. (43) can be expressed in terms of matrix $M$:

$$M \cdot M^t \cdot \vec{\lambda} = \vec{r}, \tag{47}$$

Recall the *rhs* $\vec{r} = \vec{r} = (1 + \hat{\omega}) \nabla^h p - \sum_{s=1}^{n_S} \hat{\xi}_s \nabla^c \rho_s - \nabla^c \left( \rho H - \rho e_v - \frac{\rho u^2}{2} \right)$, that can be written:

$$\vec{r} = M \cdot \left[ \begin{array}{c} -\hat{\xi}_1 \\ \cdots \\ -\hat{\xi}_{n_S} \\ 1 + \hat{\omega} \end{array} \right] - \nabla^c \left( \rho H - \rho e_v - \frac{\rho u^2}{2} \right) \equiv M \cdot \vec{r}_1 + \vec{r}_2. \tag{48}$$

Consider now a situation where the gradients of all species are aligned, *i.e.* across a normal shock wave or a contact discontinuity. In such a case:

$$\begin{aligned} \nabla^c \rho_2 &= \alpha_2 \nabla^c \rho_1, \\ &\cdots \\ \nabla^c \rho_{n_S} &= \alpha_{N-1} \nabla^c \rho_1, \\ \nabla^h p &= \alpha_N \nabla^c \rho_1, \\ \nabla^c \left( \rho H - \rho e_v - \frac{\rho u^2}{2} \right) &= \alpha_{N+1} \nabla^c \rho_1, \end{aligned} \tag{49}$$

and the coefficient matrix $\mathcal{B}$ reduces to:

$$\mathcal{B} = M \cdot M^t = \left(1 + \alpha_2^2 + \ldots + \alpha_N^2\right) \left[ \begin{array}{c} m_{x,1} \\ m_{y,1} \\ m_{z,1} \end{array} \right] \cdot [m_{x,1}\, m_{y,1}\, m_{z,1}] = \left(1 + a^2\right) \vec{m}_1 \cdot \vec{m}_1^t \tag{50}$$

Notice how the determinant of $\vec{m}_1 \cdot \vec{m}_1^t$ is zero. The *rhs* becomes in turn:

$$\vec{r} = \left( 1 + \hat{\omega} - \sum_{s=1}^{n_S} \hat{\xi}_s - \alpha_N \right) \vec{m}_1 = b\, \vec{m}_1. \tag{51}$$

The linear system is hence $\vec{m}_1 \left( \left(1+a^2\right) \vec{m}_1^t \cdot \vec{\lambda} - b \right) = 0$.
Therefore, we have shown that matrix $\mathcal{B}$ determinant is zero whenever the gradients of all the quantities ($\rho_s$, $p$, ...) are aligned: that is, whenever there is a normal shock wave or a contact on the domain, the linearization procedure leads to a situation where there might be either an $\infty$ number of solutions, or no solution at all.
The matter is further complicated if we take into account round-off errors: determinant $|\mathcal{B}|$ could be not zero but very small: the linearization procedure being extremely ill-conditioned.
In an attempt to alleviate the conditioning problem, we have applied a truncated `SVD` technique. Matrix $M$ is expressed as the product:

$$M \rightarrow L \cdot S \cdot R^t. \tag{52}$$

Matrices $L \in \mathbb{R}^{n_D \times n_D}$ and $R \in \mathbb{R}^{n_S \times n_S}$ are orthogonal, and $S \in \mathbb{R}^{n_D \times n_S}$ is the singular values matrix, consisting of non-negative entries. Substitution into Eq. (47) yields:

$$L \cdot S \cdot R^t \cdot R \cdot S^t \cdot L^t \cdot \vec{\lambda} = L \cdot S \cdot R^t \cdot \vec{r}_1 + \vec{r}_2. \tag{53}$$

Pre-multiplying by $L^t$ leads to:

$$\underbrace{S \cdot S^t}_{\Sigma} \cdot L^t \cdot \vec{\lambda} = S \cdot R^t \cdot \vec{r}_1 + L^t \cdot \vec{r}_2, \tag{54}$$

where $\Sigma$ is a diagonal matrix with non-negative entries. For the aligned-gradient case we know that at least one of the diagonal entries is zero (or very close to machine zero). We can obtain a solution $\vec{\lambda}^*$ to (54):

$$\vec{\lambda}^* = L \cdot \left(\Sigma^*\right)^{-1} \cdot \left( S \cdot R^t \cdot \vec{r}_1 + L^t \cdot \vec{r}_2 \right), \tag{55}$$

where the diagonal matrix $\left(\Sigma^*\right)^{-1}$ contains either the inverse of the eigenvalues/singular values of $\Sigma$ (that is $\frac{1}{\sigma_i^2}$) or zero (if $\sigma_i^2 < \varepsilon$), with $\varepsilon$ a threshold parameter to decide when to neglect a particular eigenvalue.
Unfortunately, the truncated `SVD` inversion was not enough to surpass the ill-posedness problems, since the threshold parameter $\varepsilon$ has to be tuned; this impacts in turn to which level the conservation restrictions Eq. (35) are fulfilled. In our experience, small errors on the conservation restrictions are enough to spoil a numerical solution.
More robust alternatives to the *TCNEQ* Roe like linearization are therefore desired: this is the reason behind the application of regularized *CRD* schemes as the one described in Eq. (29).
Along this line, reference 12 describes the application of the *Bcx* scheme in (29) regularized with additional shock dissipation in Eq. (30) and the shock detector from 15, 13 for the simulation of the inviscid flow around the mid-section of a circular cylinder ($25.4 m\,m$ in radius) placed into a hypersonic $N$-$N_2$ stream in *TCNEQ* conditions, see Table 2.
Flow tangency (inviscid wall *BC*) has been imposed at the wall, a supersonic inlet at the exterior curved boundary and supersonic outlet at the remaining boundaries. The solutions have been obtained in triangular meshes of resolution $n_T \times n_R = 242 \times 129$ nodes, *i.e.* with $n_{Elem} = 6.1 \times 10^4$ and $n_{DoF} = 3.1 \times 10^4$ degrees of freedom. Figure 6a present similar but coarser grids with $n_T \times n_R = 62 \times 33$ points. No sign of carbuncle was observed in these simulations, 11.

Table 2: Hypersonic inviscid *TCNEQ* flow around cylinder. $N - N_2$ mixture. Testcase definition.

| $Ma_\infty$ | $\rho_\infty\,[kg/m^3]$ | $u_\infty\,[m/s]$ | $T_\infty\,[K]$ | $T_{v,\infty}\,[K]$ | $y_{N,\infty}\,[-]$ | $y_{N2,\infty}\,[-]$ |
|---|---|---|---|---|---|---|
| 6.2 | $5.1512 \times 10^{-3}$ | 5590. | 1833. | 1833. | 0.9621 | 0.0379 |

Figure 6b shows the region where the shock detector is active, *i.e.* $\theta \in (0, 1]$. Note how in both cases the shock is captured across a very narrow region.
The $Bcx$ solution is restarted from a $1^{st}$ order solution obtained with the $Nc$ scheme. The residual associated to the roto-translational temperature decreases six orders of magnitude, as seen in Figures 7f.
The results are gathered in Fig. 7. Note the strong compression in Fig. 7a. The effectivity of the additional shock dissipation term Eq. (29) is evident from the the Mach number field in Fig. 7b: no overshoots of the Mach number are apparent.
Roto-translational and vibrational temperatures differ in the shock-layer, as is evident from figures 7c and 7d: the flow is in thermal non-equilibrium in the post-shock region.
High temperatures in the post-shock region result as well in the dissociation of the molecular $N_2$ into atomic nitrogen, see Fig. 7e.

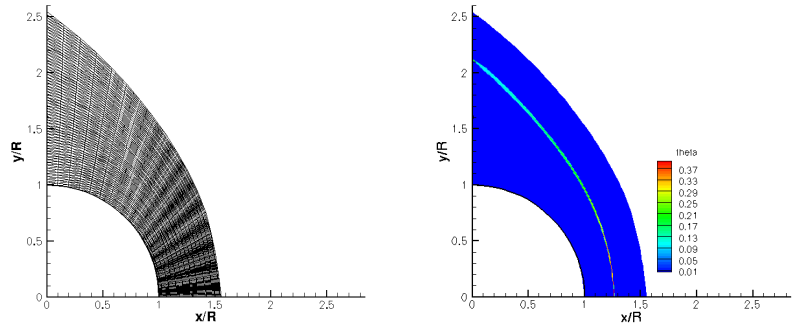


(a) Mesh. (b) Shock detector $\theta$.

Figure 6: Hypersonic inviscid *TCNEQ* flow around cylinder: in (a), mesh employed (only upper half and one out every fourth point shown); in (b): shock detector activation region.

## 5 CONCLUSIONS

In this contribution we have revisited the multidimensional extension in 8 of the generalized Roe-averaging procedure that Liu and Vinokur introduced in 22.
Specifically, we have covered the case of the hypersonic flow of gas mixtures in thermal and chemical non-equilibrium conditions. The linearization procedure has been described in detail, and an analysis of its limits of applicability has been conducted. We have shown that under some conditions the linearization procedure is not well-defined.
An alternative strategy to deal with the flows of our interested has been proposed. This strategy resorts to the application of now classical contour-integration-based residual distribution schemes. The non-positivity of such schemes is addressed with a regularization term applied across numerically captured shock waves.

## ACKNOWLEDGMENTS

First author has been supported through the NNATAC FP7 initiative (PIAP-GA-2012-324298) and the European Commission Research and Innovation action DRAGY (GA-690623).

## Appendix A Further details on Residual Distribution Schemes

This appendix presents additional details on the residual distribution solver employed in this work.

### A.1 Source term residual

The source term contribution to the nodal residual $\mathfrak{f}^S\left(\vec{\Phi}^{S,\Omega_i}\right)$ in equation (11) is derived through a variational principle applied to the source term $\vec{S}$:

$$\vec{\Phi}_l^S = \int_\Omega \omega_l \, \vec{S} dv. \tag{56}$$

Straightforward manipulations reduce previous equation to:

$$\vec{\Phi}_l^S = \int_{\Xi_l} \omega_l \, \vec{S} dv = \sum_{\Omega_i \in \Xi_l} \int_{\Omega_i} \omega_l \vec{S} dv. \tag{57}$$

If a one-point quadrature rule is employed, Eq. (57) in discrete form is:

$$\vec{\Phi}_l^S = \sum_{\Omega_i \in \Xi_l} \Omega_i \omega_l \left(\vec{x}_g\right) \vec{S}\left(\vec{x}_g\right), \tag{58}$$

where $\vec{x}_g$ is the center of mass of the simplicial element $\Omega_i$.
In this manner, it is possible to define distribution matrices for the source term:

$$B_l^{\Omega_i,S} = \frac{1}{\Omega_i} \int_{\Omega_i} \omega_l dv. \tag{59}$$

Typically, $B_l^{\Omega_i,S}$ is chosen to coincide with the distribution matrix for the advective term, if such a matrix exists. For the particular case of the $Nc$ scheme, the $LDAc$ distribution matrix is employed 25, 18.

### A.2 Boundary conditions

References 7, 2 present detailed considerations on boundary condition enforcement in the context of residual distribution schemes. Here, we discuss briefly the difference between strongly/weakly imposed boundary conditions and its relation to the limited subset of $BC$'s employed in this work.

A boundary condition is imposed *strongly* when the *a priori* known value of the solution is substituted into Eq. 9, so that:

$$\vec{U}^h(\vec{x},t) = \sum_{j\in\delta\Omega^{h,D}} \vec{U}_j^{BC} N_j(\vec{x}) + \sum_{j\in\Omega^h-\delta\Omega^{h,D}} \vec{U}_j N_j(\vec{x}). \tag{60}$$

Alternatively, $BC$'s can be enforced *weakly*, by adding a residual $\vec{\Phi}_l^{BC}$ to equation (11). This $\vec{\Phi}_l^{BC}$ is designed so that the solution $\vec{U}_l$ at steady state reduces to the requested value $\vec{U}_l^{BC}$. The rationale for this technique departs from the weak formulation of the problem:

$$\int_\Omega \omega_l \frac{\partial \vec{F}_j}{\partial x_j}\, dv = \vec{0}.$$

Integration by parts, application of Gauss-Ostrogradsky theorem, and yet again integration by parts recast the problem as:

$$\int_\Omega \omega_l \frac{\partial \vec{F}_j}{\partial x_j}\left(\vec{U}^h\right) dv + \underbrace{\oint_{\delta\Omega} \omega_l \left[\vec{F}_j\left(\vec{U}^{h,BC}\right) - \vec{F}_j\left(\vec{U}^h\right)\right] 1_j^{ext} ds}_{\vec{\Phi}_l^{BC}} = \vec{0}. \tag{61}$$

Discretization of interior points is recovered but contributions from boundary conditions is now explicit. Equation (61) can be integrated numerically, or alternatively it can be cast in linearized form:

$$\vec{\Phi}_l^{BC} = \sum_{S_f\in\delta\Xi_l\cap\delta\Omega} \int_{S_f} \omega_l^{\delta\Omega_i} A_j^{c,U}\left(\vec{U}^{h,BC} - \vec{U}^h\right) 1_j^{ext} ds = K_l\cdot\left(\vec{U}_l^{BC} - \vec{U}_l^h\right). \tag{62}$$

*RD* schemes being a vertex-centered numerical technique, strong imposition of boundary conditions is straightforward there where the solution is fully known a priori, namely for the case of supersonic inlets. Nodes on a supersonic outlet region are treated as interior points, in agreement with characteristic lines leaving the domain.
Conversely, whenever the state vector cannot be defined unambiguously neither from the interior solution nor from external information, weak enforcement of the boundary condition is the natural alternative, specially if the *upwind projector* $K_l^+$ is used in Eq. (62) instead of $K_l$. The *upwind projector* discriminates information entering the domain while discards contributions associated to outgoing characteristics: this is the principle supporting weak far-field $BC$. Inviscid walls are also enforced weakly, but through Eq. (61). The flow tangency condition is imposed by specifying:

$$\Delta\vec{F}_j^c \equiv \vec{F}_j^{c,BC} - \vec{F}_j^{c,h} = -\left[\rho\, u_n, \rho\, u_j\, u_n, \rho E\, u_n\right]^t. \tag{63}$$

Symmetry is achieved simply by setting the vertical velocity component $v$ to 0 in $\vec{U}_l^{BC}$, see 34.

### A.3 Numerical solution of the discretized set of equations

Since system of equations (1) is of mixed parabolic-hyperbolic type, 16, its steady solution can be obtained marching in pseudo-time. The distribution procedure described in sections 3.1 and A.1 leads to the definition of a system of ordinary differential equations controlling the time evolution of the solution at the grid nodes. For the $l$-th node, it reads:

$$V_{\Xi_l} \frac{d\vec{U}_l}{dt} + \vec{\Phi}_l^c - \vec{\Phi}_l^S = \vec{0}, \tag{64}$$

where $V_{\Xi_l}$ stands for the volume of the median dual cell around $l$-th node.
The discretization of Eq. (64) is accomplished by means of the `COOLFluiD` solver, described in 19. Equation (64) is marched in pseudo-time until a steady state solution is reached, by using an implicit backward Euler integrator. The linear system of equations obtained at each *pseudo-time* step is then solved by one of the Krylov subspace methods 28 provided by the `PETSc` solver library.
All thermophysical properties and non-equilibrium terms are provided by the `MUTATION` library (see 23 for more details on the physico-chemical modeling aspects). As far as boundary conditions are concerned, supersonic inlet boundary conditions are enforced strongly, whereas inviscid wall boundary conditions are imposed weakly, as detailed in 34.

## References


[1] R. Abgrall and M. Mezine. Construction of $2^{nd}$-order accurate monotone and stable rds for steady flow problems. *J. Comput. Physics*, 195:474–507, 2004. 9

[2] R. Abgrall and D. De Santis. Linear and non-linear high order accurate residual distribution schemes for the discretization of the steady compressible Navier–Stokes equations. *J. Comput. Physics*, 283:329 – 359, 2015. ISSN 0021-9991. 19

[3] A.J Chorin and Marsden J.E. *A Mathematical Introduction to Fluid Mechanics, $3^{rd}$ edition*. Springer, 2000. 3

[4] A. Csìk, M. Ricchiuto, and H. Deconinck. Conservative formulation of the multidimensional upwind residual distribution schemes for general nonlinear conservation laws. *J. Comput. Physics*, 179(1):286–312, 2002. 5, 6, 8

[5] H. Deconinck, P.L. Roe, and R. Struijs. A multidimensional generalization of Roe's flux difference splitter for the Euler equations. *Computers and Fluids*, 22(2-3):215–222, 1993. 6

[6] H. Deconinck, K. Sermeus, and R. Abgrall. Status of multidimensional upwind residual distribution schemes and applications in aeronautics. In *Proceedings of the AIAA Fluids 2000 Conference, Denver, 2000*. AIAA, 2000. 8

[7] H. Deconinck, M. Ricchiuto, and K. Sermeus. Introduction to residual distribution schemes and stabilized finite elements. LS 2003-05, VKI, 2003. 19

[8] G. Degrez and E. van der Weide. Upwind residual distribution schemes for chemical non-equilibrium flows. In *Collection of Technical Papers. Vol. 2*, pages 978–987. AIAA, 1999. 1, 2, 6, 9, 18

[9] Jiří Dobeš and Herman Deconinck. Second order blended multidimensional upwind residual distribution scheme for steady and unsteady computations. *Journal of Computational and Applied Mathematics*, 215(2):378 – 389, 2008. Proceedings of the Third International Conference on Advanced Computational Methods in Engineering (ACOMEN 2005). 8

[10] J. Garicano-Mena. *On the computation of heat flux in hypersonic flows using Residual Distribution Schemes*. PhD thesis, Université Libre de Bruxelles, 2014. 8

[11] J. Garicano-Mena, A. Lani, and H. Deconinck. An energy-dissipative remedy against carbuncle: Application to hypersonic flows around blunt bodies. *Computers and Fluids*, 133:43 – 54, 2016. ISSN 0045-7930. 9, 16

[12] J. Garicano-Mena, A. Lani, and G. Degrez. An entropy-variables-based formulation of residual distribution schemes for non-equilibrium flows. *Journal of Computational Physics*, 362:163 – 189, 2018. ISSN 0021-9991. 8, 16

[13] Jesús Garicano-Mena, Raffaele Pepe, Andrea Lani, and Herman Deconinck. Assessment of heat flux prediction capabilities of residual distribution method: Application to atmospheric entry problems. *Communications in Computational Physics*, 17:682–702, 3 2015. ISSN 1991-7120. 8, 16

[14] P. Gnoffo, R. Gupta, and J. Shinn. Conservation equations and physical models for hypersonic air flows in thermal and chemical non-equilibrium. TP 2867, NASA, 1989. 2, 3

[15] P. A. Gnoffo. Updates to multi-dimensional flux reconstruction for hypersonic simulations on tetrahedral grids. In *Proceedings of the* $48^{th}$ *AIAA Aerospace Science Meeting and Exhibit*, Orlando(FL), 2010. AIAA. 16

[16] C. Hirsch. *Numerical Computation of Internal and External Flows: Introduction to the Fundamentals of CFD,* $2^{nd}$ *Edition*. Butterworth-Heinemann, 2006. 3,

[17] J.O. Hirschfelder, C.F. Curtiss, and R.B. Bird. *The Molecular Theory of Gases and Liquids, Second edition*. Wiley, 1964. 3

[18] A. Lani. *An object oriented and high-performance platform for aerothermodynamic simulations*. PhD thesis, Université Libre de Bruxelles, 2008. 18

[19] A. Lani, N. Villedieu, K. Bensassi, L. Kapa, M. Vymazal, M. S. Yalim, and M. Panesi. COOLFluiD: an open computational platform for multi-physics simulation and research. In *AIAA 2013-2589*, San Diego (CA), Jun 2013. 21th AIAA CFD Conference.

[20] Lani, A., Panesi, M. and Deconinck, H. Conservative residual distribution method for viscous double cone flows in thermochemical nonequilibrium. *Communications in Computational Physics*, 13:479–501, 2013. 5

[21] P.D. Lax. Weak solutions of nonlinear hyperbolic equations and their numerical computation. *Communications on Pure and Applied Mathematics*, 7(1):159–193, 1954. ISSN 1097-0312. 9

[22] Y. Liu and M. Vinokur. Upwind algorithms for general thermo-chemical nonequilibrium flows. In *Proceedings of the* $27^{th}$ *AIAA Aerospace Science Meeting and Exhibit*, Reno(NV), 1989. AIAA. 1, 3, 6, 10, 18

[23] M. Panesi. *Physical models for nonequilibrium plasma flow*. PhD thesis, Universit degli studi di Pisa, 2009. 3,

[24] C. Park. *Nonequilibrium hypersonic aerothermodynamics*. Wiley-Interscience, 1990. 2

[25] M. Ricchiuto. *Construction and analysis of compact residual distribution discretizations for conservation laws on unstructured meshes*. PhD thesis, Université Libre de Bruxelles, 2005. 4, 6, 8, 18

[26] P. Roe. Linear advection schemes on triangular meshes. Coa, Cranfield Institute of Technology, 1987. 7

[27] P.L. Roe. Approximate Riemann Solvers, Parameter Vectors, and Difference Schemes. *J. Comput. Physics*, 43:357–372, 1981. 1, 6

[28] Y. Saad. *Iterative methods for sparse linear systems: Second edition*. SIAM, 2003.

[29] K. Sermeus. *Multi-Dimensional Upwind Discretization and Application to Compressible Flows*. PhD thesis, Université Libre de Bruxelles, 2013. 4, 6, 8

[30] K. Sermeus and H. Deconinck. Solution of steady euler and navier-stokes equations using residual distribution schemes. LS 2003-05, VKI, 2003. 6

[31] R. Struijs, H. Deconinck, and P. Roe. Fluctuation splitting for multidimensional convection problems: an alternative to finite volume and finite element methods. LS 1990-04, VKI, 1990. 7

[32] N. Tsuboi, A.K. Hayashi, and Y. Matsumoto. Three-dimensional parallel simulation of cornstarch-oxygen two-phase detonation. *Shock Waves*, 10:277–285, 2000. 1

[33] Nobuyuki Tsuboi, Makoto Asahara, Keitaro Eto, and A. Koichi Hayashi. Numerical simulation of spinning detonation in square tube. *Shock Waves*, 18:329–344, 2008. 1

[34] E. van der Weide. *Compressible flow simulation on unstructured grids using multi-dimensional upwind schemes*. PhD thesis, Technische Universitet Delft, 1998. 1, 4, 7, 19,

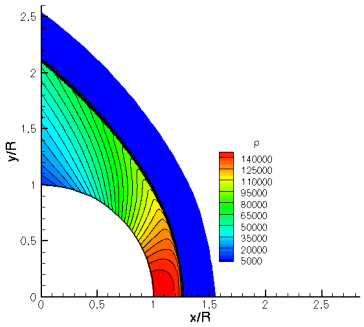


(a) Pressure field ($Pa$).

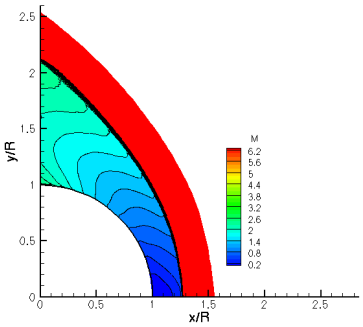


(b) $Ma$ field.

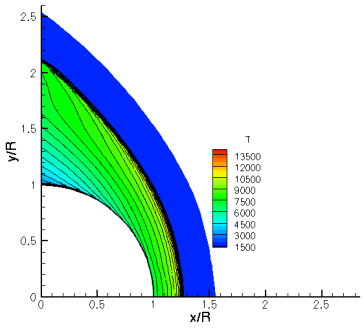


(c) $T$ field ($K$).

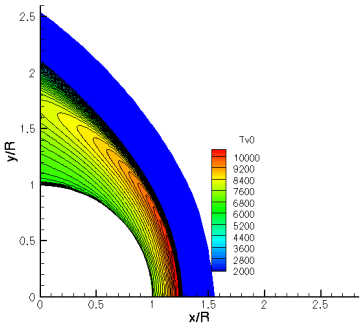


(d) $T^v$ field ($K$).

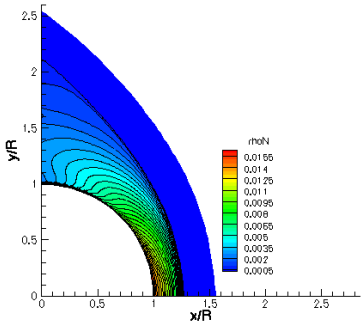


(e) $\rho_N$ field ($^{kg}/_{m^3}$).

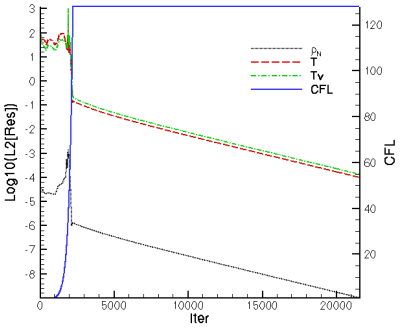


(f) Convergence history.

Figure 7: Hypersonic inviscid *TCNEQ* flow around cylinder. $N - N_2$ mixture.